

Mechanical properties of the elemental nanocomponents of nacre structure

Ph. Stempflé ^{a)*}, O. Pantalé ^{b)}, M. Rousseau ^{c)}, E. Lopez ^{d)}, X. Bourrat ^{e)}

- a) Corresponding author : Institut FEMTO-ST (UMR CNRS 6174 – Université de Franche Comté – CNRS – ENSMM – UTBM), ENSMM, 26 chemin de l'Épitaphe, F – 25030 Besançon Cedex, France +33 (0) 3 81 40 27 64 philippe.stempfle@ens2m.fr
- b) Université de Toulouse, INP/ENIT, Laboratoire Génie de Production, 47 avenue d'Azereix, F- 65013 Tarbes, France
- c) Nancy University, UMR CNRS 7561, 9 avenue de la forêt de Haye, F-54505 Vandoeuvre les Nancy, France
- d) Muséum National d'Histoire Naturelle, UMR 5178 CNRS – MNHN, CP 26, 43 Rue Cuvier, F-75005, Paris, France
- e) Université d'Orléans, CNRS ISTO, 1A Rue de la Férollerie, F-45071 Orléans cedex 2, France

Sheet nacre is a nanocomposite with a multiscale structure displaying a lamellar “bricks and mortar” microarchitecture. In this latter, the brick refer to aragonite platelets and the mortar to a soft organic biopolymer. However, it appears that each brick is also a nanocomposite constituted as CaCO₃ nanoparticles reinforced organic composite material. What is the role of this “intracrystalline” organic phase in the deformation of platelet? How does this nanostructure control the mechanical behaviour of sheet nacre at the macroscale? To answer these questions, the mechanical properties of each nanocomponents are successively investigated and computed using spherical and sharp nanoindentation tests combined with a structural model of the organomineral platelets built from AFM investigations.

Keywords: mother of pearl, nanoindentation, AFM Image analysis, biocrystals, aragonite platelets

1. Introduction

Nacre is a natural nanocomposite currently studied in many fields essentially for designing organic/inorganic materials, improving properties or understanding self-assembling nanophases at ambient temperature [1-3]. The mechanical properties of nacre have long been studied following a simplistic “bricks and mortar” composite model (fig. 1). This was based on the idea that nacre aragonite platelets behave like “brittle stiff bricks” (97 wt.%) and the “intercrystalline” organic phase (3 wt.%) like a “compliant mortar” (fig. 2). Thus, nacre intrinsic mechanical properties are usually deduced considering a lamellar micro-architecture [4-6] by combining organic [7-9] and crystalline aragonite [10, 11]. Although sufficient to explain deformation and fracture mechanisms of sheet nacre under *quasi-static* solicitations (fig. 1) on the micro- and macroscale [12-15], this model does not enable to explain the particular mechanical behaviours which occur under *dynamic* solicitations [16, 17]. Indeed, these latter directly involve the nanostructure of the platelet and require a better knowledge of the mechanical properties of the individual platelet.

In agreement with other groups [18-22], nanoindentation and near field microscopy are the suitable tools to address this issue because of the heterogeneity of nacre nanostructure. Thus, first evidences of ductile behaviour of platelet – involving the presence of nanograins [21] and their mobility mechanism [22] – were yielded by several authors using both nanoindentation [19, 20] and AFM [21, 22]. Unfortunately, these authors produced only surface evidences of nanograins which were sometimes interpreted as the platelet's roughness [19, 20].

Aragonite platelet clearly revealed its 3D nanogranular structure embedded by an “*intracrystalline*” organic matrix as demonstrated in 2005 [16] flat-on (fig. 3) and confirmed in cross section views (fig. 4) [23, 24]. The presence of nanograins as a nanostructure of platelets was clearly confirmed by different groups combining several approaches [17, 23-25, 27, 28, 31]. First, NMR has suggested the chemical bonding reality between organic and mineral within the platelet [32]. Also high resolution and dark-field TEM technique has evidenced the crystallinity of the “*intracrystalline*” organic network inside the “mineral” crystal [32, 33]. Finally, friction mechanical behaviour at platelet level was seen in complete agreement with this nanograined-structure [16, 17, 27]. On the basis of these different results, platelet was described, for the first time as a “*pseudo*” single crystal – *i.e* an organomineral composite made up with aragonite nanograins all coherently oriented regarding diffraction and embedded in a crystallized organic phase [23, 24]. This nanostructure refers to the heteroepitaxial growth model reported by Weiner *et al* [26].

Hence, nacre possesses a double composite structure at two orders of magnitude, represented in the schematic of fig. 5 from [16] published back in 2006. The organic matrix is the “*continuous phase*” at both scales with different properties in-between or inside the tablets but with strong connections. This *multiscale* structure implies that nacre behaves in different manners depending on the mechanical solicitation. Thus for *quasi-static* mechanical tests (see fig. 1) the fracture is rather localized along the interface between adjacent platelets within the “*intercrystalline*” organic matrix [4-6, 12-15]. On the contrary, under *dynamic* solicitation like tribological tests [16, 17, 27], fracture generally occurs inside the platelets itself – involving the fracturing of the “*intracrystalline*” organic matrix [16] by friction-induced nanoshocks [17] and thermal effects [27]. This is statistically observed by AFM views of the fracture plane of a platelet (fig 6a). Indeed, successive enlargements of the crumbled edge line clearly reveal that the platelet appears as a CaCO₃ nanoparticles reinforced organic composite material (fig. 6b). The so-called sheet nacre's aragonite platelet is in fact an organomineral platelet where the mechanical properties of each elemental phase remain largely unknown. Thus, although many works were carried out to elucidate the mechanical behaviour of nacre [4-6, 12-15, 18-20], too few works have been made to really link it to its elemental nanocomponents – *i.e* biocrystals and “*intracrystalline*” organic phase – in order to build a *multiscale* mechanical approach of sheet nacre.

The aim of the present paper is the evaluation of the mechanical properties of those elemental nanocomponents from the organomineral platelet's mechanical properties assessed by the combined use of nanoindentation and a structural model deduced from the AFM image analysis. For this purpose, two diamond indenters were used: a 5µm radius spherical indenter suitable to evaluate the elastic properties of the aragonite platelets [17] and a three-sided Berkovich pyramid indenter more appropriate to isolate the mechanical properties of the nanograins [28]. The structural model results from the Mori-Tanaka's theory [29] improved by the works of Benveniste allowing the effective computation of the nanocomposite's mechanical properties [30]

2. Experimental

2.1. Samples

Samples are made of sheet nacre extracted from giant oyster *Pinctada maxima* [16, 25]. They are polished more or less parallel to the aragonite platelets : size: 5 μm , thickness: 400 nm, $R_a = 14 \pm 0.6$ nm (fig. 5a). Other details about these samples are available in [16, 17, 23, 27]

2.2. Atomic Force Microscopy & image analysis

Topography is assessed using an AFM Dimension 3000 connected to a Nanoscope IIIa electronic controller (*Digital Instruments Santa Barbara USA*). Its spatial and vertical resolution are lower than 1 nm and the field depth is in-between 100 nm and 100 μm . Maps were achieved at high resolution (512 \times 512 pixels) using an intermittent contact mode (so-called TappingMode™). The silicon nitride probe displays a tip rounding lower than 10 nm. The work frequency, the stiffness and the cantilever amplitude are respectively: 270 kHz, 42 Nm^{-1} and 25 nm. According to the size of the images (between 0.25 μm^2 and 25 μm^2) the scanning rates varies from 1 $\mu\text{m}\cdot\text{s}^{-1}$ to 2.4 $\mu\text{m}\cdot\text{s}^{-1}$.

The size, the shape and the volume fraction of the initial biocrystal nanograins were determined from the phase contrast maps (fig. 7) with a specific algorithm developed for the SPM data analysis software Gwyddion (www.gwyddion.net). Analysis was made from cumulated measurements of at least 5,000 particles (images of 0.25 – 1 μm^2) in order to satisfy a statistical validity. The average size of the nanograins is 38 ± 21 nm, their distribution in size is reported in fig.7. The thickness of the “*intracrystalline*” matrix is about 4 nm (see fig. 3b) and its average volume fraction V_m – evaluated for a covered area about 10 μm^2 – is about 12% in 2D corresponding to 4.2% in 3D. This value is close to the one obtained by biochemical extractions [31].

2.3. Nanoindentation

Nanomechanical properties are obtained with a NHT nanoindenter (*CSM Instruments, Peseux Switzerland*). The vertical displacement and loading resolutions are respectively 0.03 nm and 1 μN . The compliance of the apparatus is 0.25 $\text{nm}\cdot\text{mN}^{-1}$. Two diamond indenters were used ($E_i = 1141$ GPa, $\nu_i = 0.07$): a 5 μm radius spherical indenter and a three-sided Berkovich pyramid indenter with a tip radius evaluated about 350 nm [28]. A minimum of 30 indentations is carried out for each test.

3. Results and discussion

3.1. Spherical nanoindentation tests

Spherical nanoindentation tests are carried out under various maximal normal loads in the range from 2 mN to 20 mN (fig 8a-c). At low loading (2 mN), the indentation depth is largely less than the platelet's thickness (400 nm) therefore the purely elastic behaviour displayed by the load-depth curves (fig. 8a) corresponds only to the one of the platelet. *Hertzian* analytical solution (fig. 8d) fitted onto the experimental curves provides the average value of the organomineral platelets ($E_p = 62.5 \pm 11.2$ GPa).

When the normal load increases (10 mN) a dissipative component appears under the load-depth curves (fig. 8b). In contrast to what is observed for mineral aragonite (without organic

matrix), no fracture-induced pop-in event is noticeable on the load-depth curve. However, piling-up phenomena are clearly observed around the indents revealing a plastic deformation probably due to the “*intracrystalline*” organic matrix: the platelet is not purely brittle but displays a ductile behaviour as reported in [19-21, 28, 35]. Then, the limit of the elastic domain – *i.e* the compressive yield stress – can be estimated from the previous *Hertzian* model as plotted in fig. 8e (about $\sigma_y = 2.7 \pm 0.7$ GPa).

When the normal load is increased up to 20 mN (fig. 8c), the contribution of the “*intercrystalline*” matrix is clearly observed because the penetration depth becomes close to the platelet’s thickness (400 nm). Thus, the Young’s modulus decreases from 62.5 to 54.4 GPa corresponding to the one of the sheet nacre ($E_N = 54.42 \pm 3.2$ GPa) [17]. Table 1 gives the elastic and dissipative contributions of the deformation energy computed from the various load-depth curves. This confirms that the elastic contribution slightly increases when the “*intercrystalline*” organic matrix is solicited beyond 10 mN.

3.2. Sharp nanoindentation tests

Results of the sharp nanoindentation tests using a Berkovich indenter are plotted in fig. 9a. The load-depth curves are strongly disturbed by the natural nanostructure of the platelets – *i.e* biocrystal nanograins. The pile-up phenomenon due to the plastic deformation is always present whatever load is applied [19, 20]. According to [17, 18], the extraction of the mechanical properties using the classical Oliver & Pharr’s method [34] is not really reliable in this case, hence the initial Oliver & Pharr Young’s modules were refined by using numerical elastic models fitted onto the beginning of the loading curves as shown in fig. 9b. For this purpose, the tip radius of the indenter has been evaluated about 350 nm [28]: $E_B = 96.75 \pm 5.67$ GPa and $\sigma_B = 13.4 \pm 2.1$ GPa. These latter are higher than those of the aragonite platelets (62 GPa) but are very close to the one of the cleaved mineral aragonite determined by nanoindentation ($E_{\text{mineral aragonite}} = 101.8 \pm 13.2$ GPa). This result is in good agreement with the one reported by Li *et al* [35] where they demonstrated – using a FFT analysis – that these nanoparticles are aragonite. These mechanical properties are also similar to the ones reported by Bruet *et al* [20] for *Trochus niloticus* nacre platelet. However, these latter attributed these values to the properties of the aragonite platelets – assumed as a single monocrystal – whereas ours results – *i.e* the comparison between spherical and sharp nanoindentation tests – rather reveal that the sharp nanoindentation tests yields the mechanical properties at the scale of the biocrystals.

3.3. Mechanical properties of the elemental nanocomponents of the organomineral platelets

Knowing the elastic properties of the platelets – as a composite nanomaterial – and the ones of the biocrystals, the mechanical properties of the “*intracrystalline*” organic phase can be computed using a suitable structural model of the organomineral platelet and the theory of homogenization. AFM is a suitable tool for establishing this structural model by combining cross sectional views (fig 4) and top views (fig 3) of the platelet. Thus, the platelet clearly appears as a nanocomposite material where mineral nanoballs are drowned into a continuous organic matrix. According to Li *et al* [35], the assembly mechanism of the aragonite nanoparticles inside individual platelets seems to be driven by amorphous aggregation and dislocation process during the biomineralization process. Keeping these considerations in mind, several assumptions can then be made about the structure of the platelet for the purpose of the modelling: (i) mineral nanograins are supposed spherical and harder than the organic

matrix; (ii) each phase can be assumed homogeneous and isotropic. Hence, the elastic properties – respectively the compression modulus K_p and the shear modulus μ_p – of this composite platelet are quite well described by the Mori-Tanaka's model [29, 30] given by the following relations (the subscripts m , b and p respectively refer to the “*intracrystalline*” matrix, the biocrystals and the platelet nanocomposite):

$$K_p = K_m + \frac{V_b K_m (K_b - K_m)}{K_m + (1 - V_b) \alpha_m (K_b - K_m)} \quad (1)$$

$$\mu_p = \mu_m + \frac{V_b \mu_m (\mu_b - \mu_m)}{\mu_m + (1 - V_b) \beta_m (\mu_b - \mu_m)} \quad (2)$$

$$\text{Where } \alpha_m = \frac{3K_m}{3K_m + 4\mu_m} \quad \beta_m = \frac{6(K_m + 2\mu_m)}{5(3K_m + 4\mu_m)} \quad (3)$$

The classical relation linking the compression and shear modules with the Young's modulus and Poisson's ratio are reminded below:

$$K_i = \frac{E_i}{3(1 - 2\nu_i)} \quad \mu_i = \frac{E_i}{2(1 + \nu_i)} \quad (i = m, b, p)$$

V_b refers to the volume fraction of nanograins computed from the one of the organic matrix assuming that there is no void or pore within the platelet ($V_b + V_m = 1$). V_m is assessed – as presented in *section 2* – by image analysis on AFM maps in phase contrast (fig. 7). Details and complete hypotheses of this model are available in [30]. Since the Poisson's ratio of either the biocrystals or the “*intracrystalline*” organic matrix are relatively invariant in comparison with the Young's modules, their values are chosen as parameters for solving this set of equations with the mathematical computing software Maxima 5.18 (<http://maxima.sourceforge.net>).

Numerical results compiled in Table 2 show that the “*intracrystalline*” organic matrix is almost 2 times less rigid than the “*intercrystalline*” organic matrix computed elsewhere [17]. In contrast to the conclusion reported by Barthelat *et al* [18], our results reveal that the “*intracrystalline*” organic phase strongly influences the behaviour of the platelets. This should enable to explain the elastoplastic behaviour of the aragonite platelets observed by nanoindentation and reported by several authors [19-22]. For instance, the effect of interactions of randomly-sized nanograins on the Poisson's ratio of the platelet – as proposed by Li *et al* [22] for explaining the plastic behaviour of grains – can be now evaluated using a discrete elements model (*e.g.* Movable Cellular Automata [36]) including the mechanical properties of each phase compiled in Table 2. Thus, these elemental properties can be used for modelling the sheet nacre with a *multiscale* approach from nanograins to the lamellar structure.

4. Conclusion

This work concerns the evaluation of the mechanical properties of the sheet nacre elemental nanocomponents constituting the organomineral platelets – *i.e.* nanograins +

“*intracrystalline*” organic matrix. Experimental characterization and numerical simulation have shown that:

- Spherical nanoindentation provides a good approximation of the platelets mechanical properties whereas sharp nanoindentation rather gives the mechanical properties of biocrystal nanograins which are greatly harder than the CaCO₃ platelets. Their high yield stress proves that they cannot easily buckle plastically. Hence, the plastic deformation of the platelet is only due to the “*intracrystalline*” matrix.
- AFM image analysis enables to study the nanostructure of the aragonite platelets: shape, size and arrangement of the aragonite nanograins within the organomineral platelet.
- The identified elastic properties of the “*intracrystalline*” organic matrix were found to be 2 times lower than those of the “*intercrystalline*” one. This probably explains the purely elastic behaviour of the platelet at low loads and the piling-up effect observed at high loads. Thus, this “*intracrystalline*” organic matrix plays a significant role in the deformation of the platelet and therefore in the deformation of the sheet nacre.

ACKNOWLEDGMENTS

The authors thank *Tahiti Perles Company* and its Chairman Robert Wan for having supplied them with the best nacre quality.

REFERENCES

- [1] S. Weiner and L. Addadi, *J. Mater. Chem.* 7, 5, (1997), 689.
- [2] M. Rousseau, A. Meibom, M. Gèze, X. Bourrat, M. Angellier, E. Lopez, *J. Struct. Biology*, 165, 3, (2009), 190.
- [3] J. Carlson, S. Ghaey, S. Moran, C.A. Tran, D.L. Kaplan, in Y. Bar-Cohen (Ed.): *Biomimetics, Biologically Inspired Technologies*, CRC Taylor & Francis, (2006), 365-379, ISBN 10:0-8493-3163-3.
- [4] R.Z. Wang, Z. Suo, A.G. Evans, N. Yao, I.A. Aksay, *J. Mater. Res.*, 16, 9, (2001), 2485.
- [5] B. Ji, H. Gao, *J. Mech. Phys. Solids*, 52, (2004), 1963.
- [6] N. M. Neves, J. F. Mano, *Mater. Sci. Eng. C*, 25, 2, (2005), 113.
- [7] G. Falini, S. Weiner, L. Addadi, *Calcif Tissue Int*, 72, (2003), 548.
- [8] F. Song, X.H. Zang, Y.L. Bai, *J. Mater Res*, 17, 7, (2002), 1567.
- [9] F. Song, A.K. Soh, Y.L. Bai, *Biomaterials*, 24, (2003), 3623.
- [10] Q.L. Feng, H.B. Li, F.Z. Cui, H.D. Li, T.N. Kim, *J. Mater. Sci Lett.*, 18, (1999), 1547.
- [11] M. Sarikaya, K.E. Gunnison, M. Yasrebi, I.A. Aksay, *Mater Res Soc Symp Proc*, 174, (1990), 109.
- [12] R.Z. Wang, H.B. Wen, F.Z. Cui, H.B. Zhang, H.D. Li, *J. Mater Sci*, 30, (1995), 2299.
- [13] S.P. Kotha, Y. Li, N. Guzelsu, *J. Mater Sci*, 36, (2001), 2001.
- [14] K. Okumura, P.G. de Gennes, *Eur. Phys J E*, 4, 1, (2001), 121.
- [15] A.G. Evans, Z. Suo, R.Z. Wang, I.A. Aksay, M.Y. He, J.W. Hutchinson, *J. Mater Res.* 16, 9, (2001), 2475.
- [16] Ph. Stempflé, M. Brendlé, *Tribology International*, 39, (2006), 1485.

- [17] Ph. Stempflé, O. Pantalé, R. Kouitat Njiwa, M. Rousseau, X. Bourrat, *Int. J. Nanotechnology*, 4, 6, (2007), 712.
- [18] F. Barthelat, H.D. Espinosa, *Proc. Of the 2003 SEM ACEEAM 2003*, June 2-4, Charlotte, North Carolina, Session 68, paper 187, (2003)
- [19] H.J. Qi, B.J. F. Bruet, J.S. Palmer, C. Ortiz, M.C. Boyce, in G.A. Holzapfel, R.W. Ogden (Eds.), *Mechanics of Biological Tissue*, Springer Berlin, Heidelberg, (2006), 189, ISBN: 978-3-54025194-1;
- [20] B.J.F. Bruet, H.J. Qi, M.C. Boyce, R. Panas, K. Tai, L. Frick, C. Ortiz, *J. Mater. Res.*, 20, 9, (2005), 2400.
- [21] X.D. Li, W.C. Chang, Y.J. Chao, R.Z. Wang, M. Chang, *Nanoletters*, 4, 4, (2004), 613.
- [22] X.D. Li, Z-H. Xu, R. Wang, *Nanoletters*, 6, 10, (2006), 2301.
- [23] M. Rousseau, E. Lopez, Ph. Stempflé, M. Brendlé, L. Franke, A. Guette, R. Naslain, X. Bourrat, *Biomaterials*, 26, 31, (2005), 6254.
- [24] M. Rousseau, X. Bourrat, Ph. Stempflé, M. Brendlé, E. Lopez, *Key. Engi. Mater*, 284-286, (2006), 705.
- [25] M. Rousseau, E. Lopez, A. Couté, G. Mascarel, D.C Smith, R. Naslain, X. Bourrat, *J. Structural Biology*, 49, (2005), 149.
- [26] S. Weiner, W. Traub, *FEBS Lett.* 111(2), (1980), 311;
- [27] Ph. Stempflé, T. Djilali, R. Kouitat Njiwa, M. Rousseau, E. Lopez, X. Bourrat, *Tribology Letters*, vol. 35, no. 2, (2009), pp. 97-104;
- [28] Ph. Stempflé, O. Pantalé, R. Kouitat Njiwa, M. Rousseau, E. Lopez, X. Bourrat, in W.J. Bartz, F. Franek, *Proc. of the 2nd Vienna International Conference of Micro-Nanotechnology*, (2007), 153, ISBN 978-3-901657-25-2,
- [29] T. Mori, K. Tanaka, *Acta Metal*, 21, (1973), 571
- [30] Y. Benveniste, *Mechanics of Materials*, 6, (1987), 147.
- [31] X. Bourrat, L. Franck, E. Lopez, M. Rousseau, Ph. Stempflé, M. Angellier, P. Alberic, *CrystEngComm*, 12,9, (2007), 1205.
- [32] K. Takahashia, H. Yamamotoa, A. Onodaa, M. Doia, T. Inabab, M. Chibab, A. Kobayashic, T. Taguchic, T. Okamuraa, N. Ueyama, *Chemical Communications*, (2004), DOI: [10.1039/b315478e](https://doi.org/10.1039/b315478e).
- [33] X. Bourrat, M. Rousseau, E. Lopez, A. Couté, G. Mascarel, D. C. Smith, P. Stempflé, 9th International Symposium on Biomineralization, 6 - 9 December 2005 Pucon, Chile (2005) <http://hal-insu.archives-ouvertes.fr/docs/00/09/20/27/PDF/Bourrat-BioMin-2005.pdf>
- [34] W.C. Oliver, G.M. Pharr, *J. Mater. Res.*, 7, 4, (1992), 1564.
- [35] X. Li, Z. Huang, *Phys. Rev. Lett.*, 102, 075502, (2009),
- [36] S. G. Psakhie, Y. Horie, G.P. Ostermeyer, S. Yu Korostelev, A. Yu Smolin, E.V. Shilko, A.I. Dmitriev, S. Blatnik, M. Spegel, S. Zavsek, *Theor. Appl. Fract. Mech.*, 1-3, (2001), 311.

FIGURES

Figure 1: Crack propagation following a tablet sliding mechanism of the nacre “bricks and mortar” structure (SEM picture after a three point bending test).

Figure 2: Typical TEM view of the microarchitecture of sheet nacre revealing the *intercrystalline* organic phase.

Figure 3: Typical AFM view of a polished surface: (left) topographic and (right) phase contrast mode of the same area.

Figure 4: SEM and AFM cross section of the organomineral platelets revealing their internal structure as a nanocomposite where mineral nanoballs are drowned into a continuous organic matrix.

Figure 5: Schematic showing the multiscale structure from nano- to macro-scale involved in the friction test, reprint from [16].

Figure 6: a) Typical AFM view of the friction track revealing the crumbling of the aragonite platelets by the presence of nanoshocks; b) cross-section revealing the internal arrangement of the nanocrystals.

Figure 7: AFM image analysis applied on the organomineral platelets for determining the size, the shape and the volume fraction of the initial platelet’s nanocomponents – i.e. nanocrystals and “*intracrystalline*” matrix.

Figure 8: Experimental load-depth curves performed with a 5 μ m spherical indenter on the organomineral platelets at respectively: a) 2mN, b) 10mN and c) 20mN; d) and e) Typical load-depth curve and numerical Hertzian model providing the elastic properties of the platelet for each test.

Figure 9: a) Experimental load-depth curves performed with a Berkovich indenter (tip radius 350nm) on the organomineral platelets and b) numerical elastic model providing the elastic properties of biocrystal nanograins.

Table 1: Evolution of the elastic and dissipative contributions of the deformation energy vs. the load in spherical nanoindentation ;

Table 2: Mechanical properties of sheet nacre and organomineral platelets nanocomponents

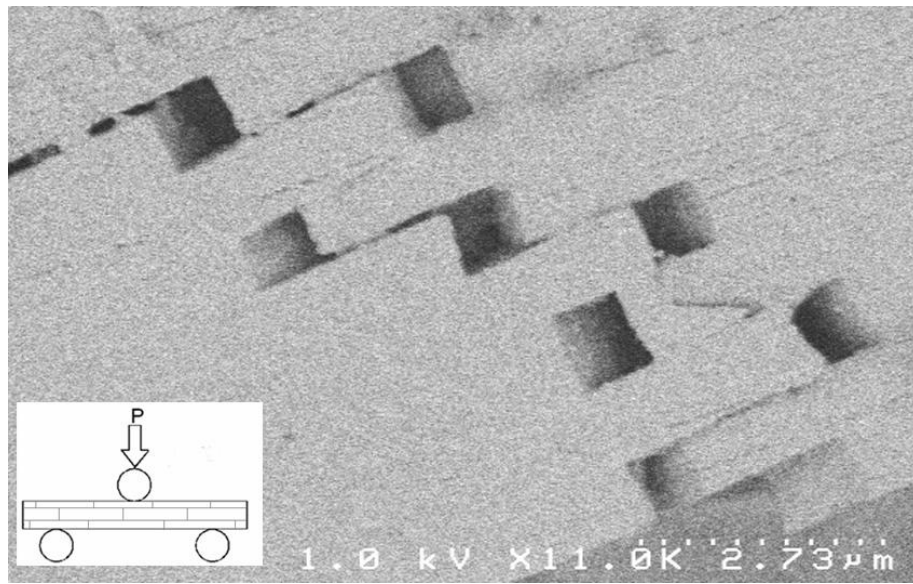


Figure 1

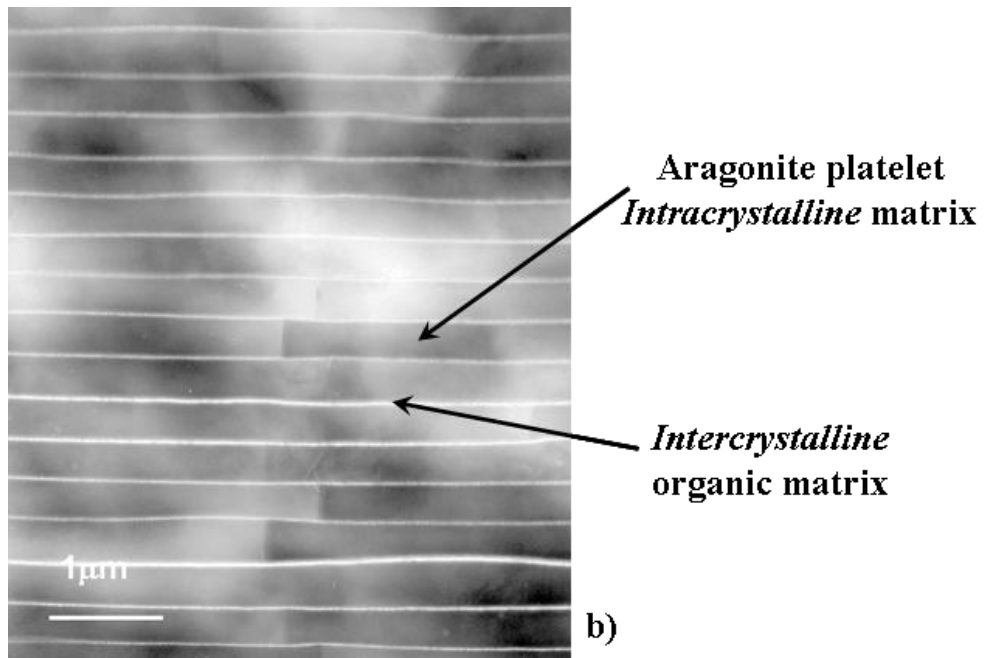


Figure 2

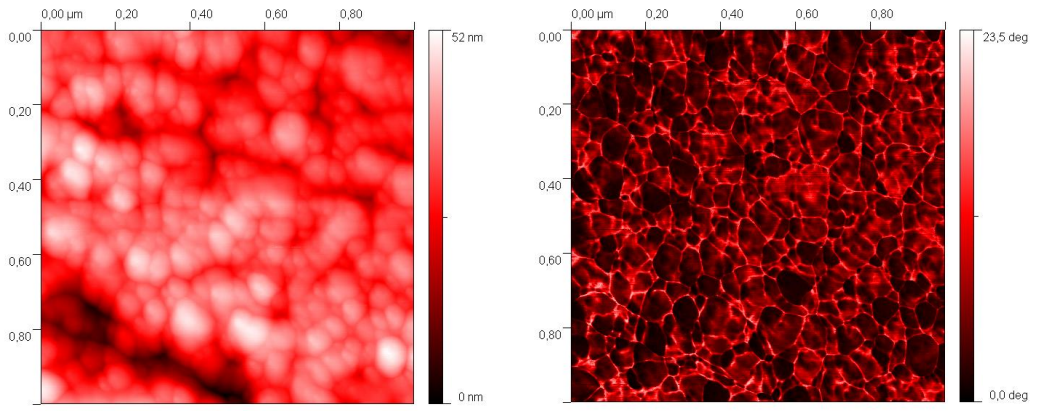


Figure 3

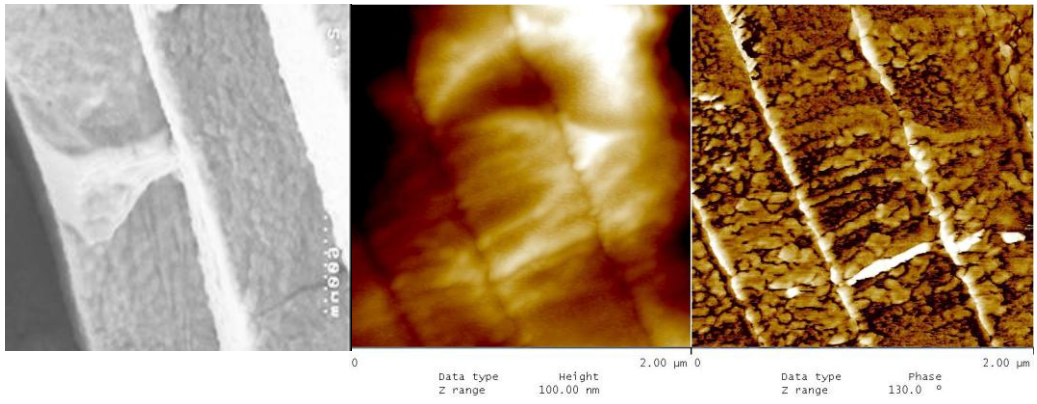


Figure 4

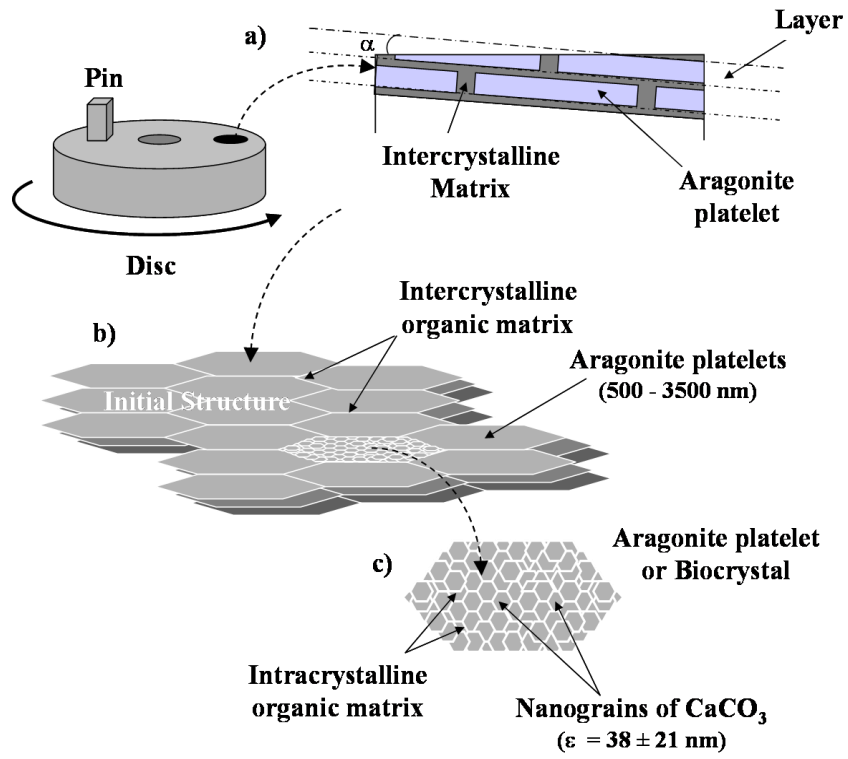


Figure 5

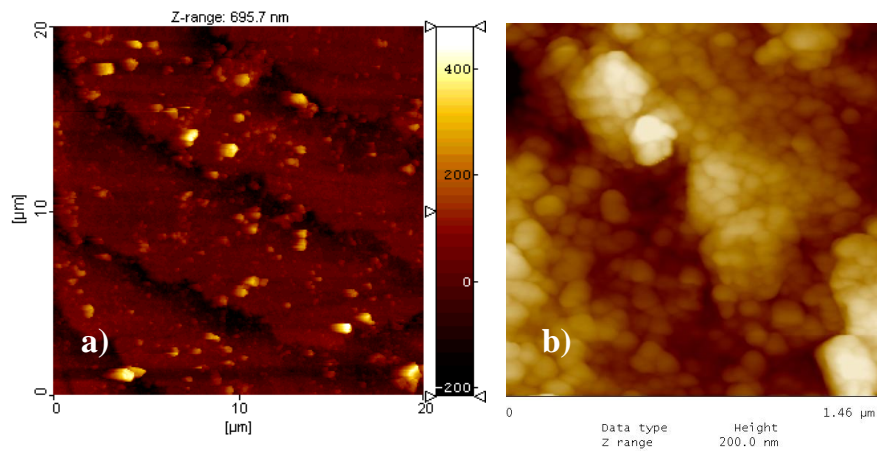


Figure 6

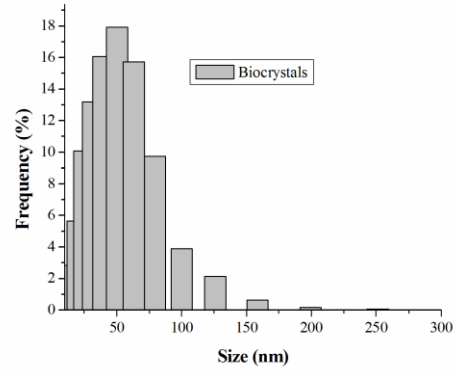
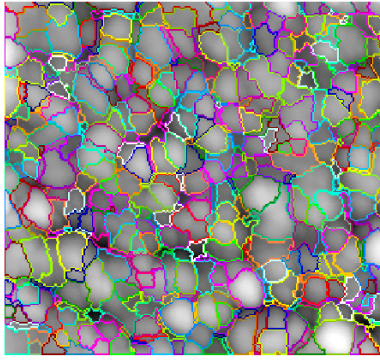


Figure 7

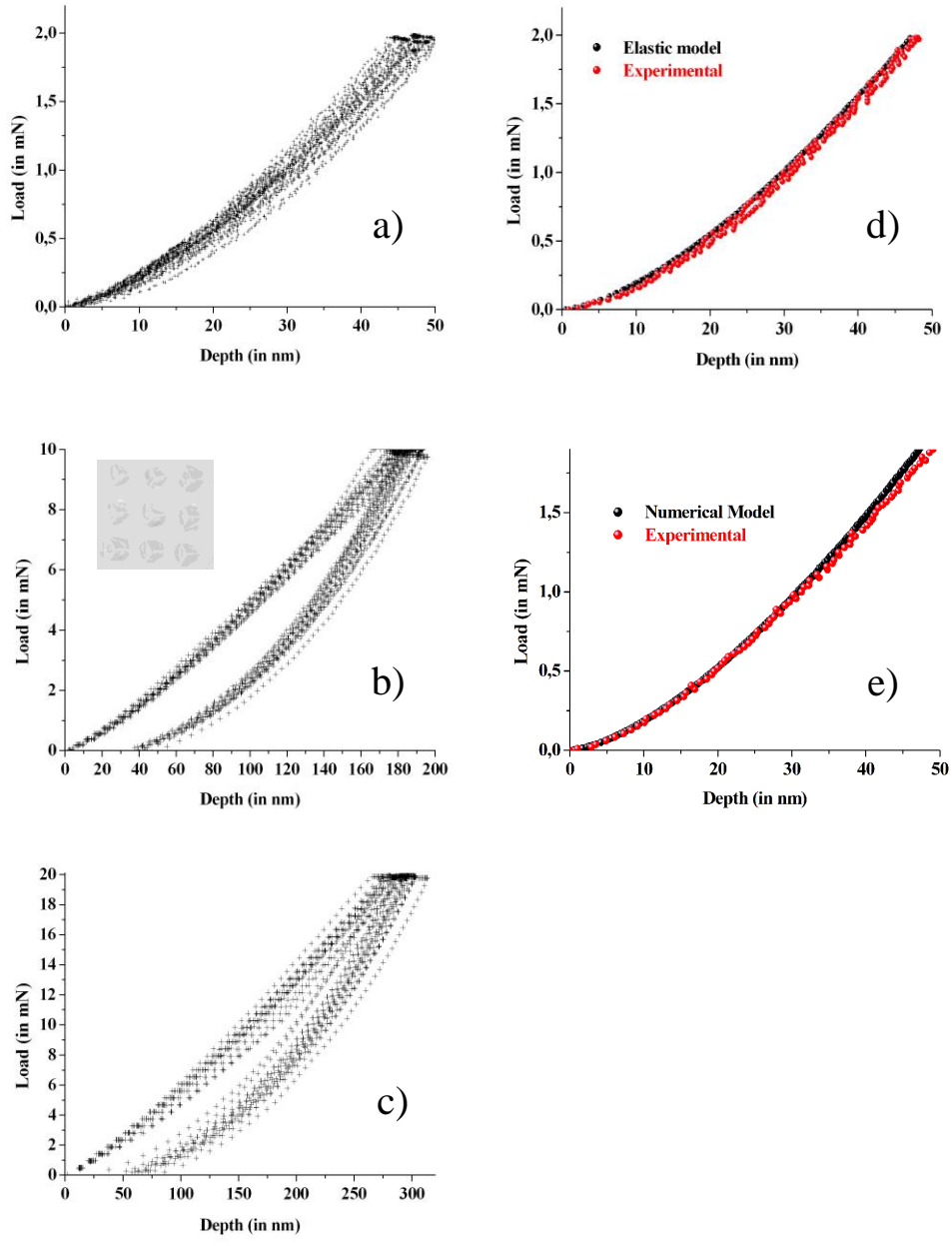


Figure 8

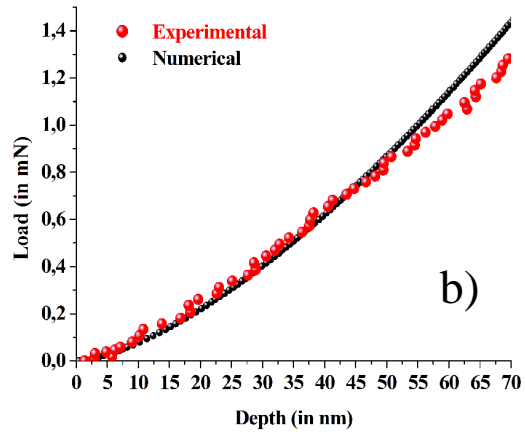
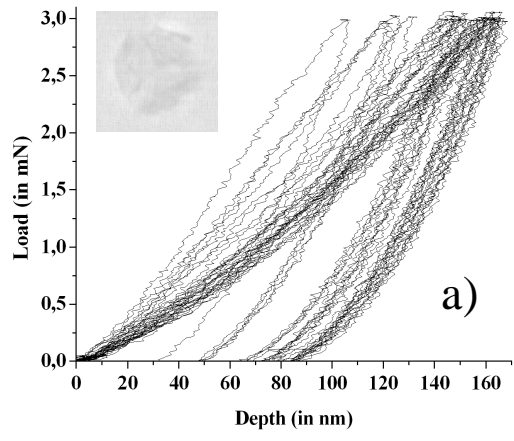


Figure 9

	2 mN	10 mN	20 mN
Elastic contribution (in %)	91.3	62.7	67.2
Dissipative contribution (in %)	8.7	37.3	34.8

Table 1: Evolution of the elastic and dissipative contributions of the deformation energy vs. the load in spherical nanoindentation

	E (GPa)	ν	σ_y (GPa)
Organomineral Platelets	62.5 (11.2) ^{c)}	0.2 (0.03) ^{c)}	2.7 (0.7) ^{b)}
Aragonite biocrystal nanograins	96.75 (5.67) ^{d)}	0.17 (0.05)^{a)}	13.4 (2.1) ^{b)}
“Intercrystalline” organic matrix^[17]	6.3 (0.56)	0.29 (1.2e-3)	-
“Intracrystalline” organic matrix	3.81 (0.41)^{a)}	0.296 (1.4e-3)^{a)}	-
Nacre lamellar microarchitecture	54.42 (3.2) ^{c)}	0.25 (0.03) ^{c)}	-

a) computed by the Mori-Tanaka model

b) computed by a *Hertzian* model

c) assessed by spherical nanoindentation test

d) assessed by sharp nanoindentation test

Table 2: Mechanical properties of sheet nacre and organomineral platelets nanocomponents